NANO LETTERS

pubs.acs.org/NanoLett Letter

Tunable Room-Temperature Ferromagnetism in Two-Dimensional Cr_2Te_3

Yao Wen, Zhehong Liu, Yu Zhang, Congxin Xia, Baoxing Zhai, Xinhui Zhang, Guihao Zhai, Chao Shen, Peng He, Ruiqing Cheng, Lei Yin, Yuyu Yao, Marshet Getaye Sendeku, Zhenxing Wang, Xubing Ye, Chuansheng Liu, Chao Jiang, Chongxin Shan, Youwen Long,* and Jun He*

Cite This: *Nano Lett.* 2020, 20, 3130−3139 Read Online

ACCESS | Metrics & More | Article Recommendations | Supporting Information

ABSTRACT: The manipulation of magnetism provides a unique opportunity for the development of data storage and spintronic applications. Until now, electrical control, pressure tuning, stacking structure dependence, and nanoscale engineering have been realized. However, as the dimensions are decreased, the decrease of the ferromagnetism phase transition temperature (T_c) is a universal trend in ferromagnets. Here, we make a breakthrough to realize the synthesis of 1 and 2 unit cell (UC) Cr_2Te_3 and discover a room-temperature ferromagnetism in two-dimensional Cr_2Te_3. The newly observed T_c increases strongly from 160 K in the thick flake (40.3 nm) to 280 K in 6 UC Cr_2Te_3 (7.1 nm). The magnetization and anomalous Hall effect measurements provided unambiguous evidence for the existence of spontaneous magnetization at room temperature. The theoretical model revealed that the reconstruction of Cr_2Te_3 could result in anomalous thickness-dependent T_c. This dimension tuning method opens up a new avenue for manipulation of ferromagnetism.

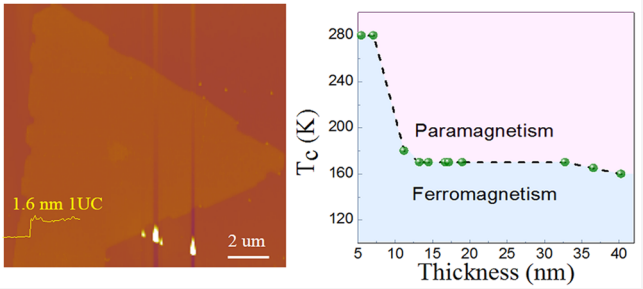

KEYWORDS: *Room-temperature ferromagnetism, anomalous Hall effect, 1 unit cell, reconstruction*

The 2D ferromagnet, as an essential part of the 2D material family, has gained attention due to their unique properties for spintronic devices. However, the thermal fluctuations will prohibit long-range ferromagnetic order in 2D isotropic Heisenberg models based on the Mermin−Wagner theorem.[1] The defect-induced magnetism based on nonmagnetic graphene has been extensively researched.[2,3] Recent reports have revealed the intrinsic long-range ferromagnetic order in atomically thin insulating $Cr_2Ge_2Te_6$,[4] CrI_3,[5] and metallic Fe_3GeTe_2[6,7] and VSe_2,[8] which initiated fundamental studies of 2D ferromagnetism. The manipulation of ferromagnetism is an attractive topic for exploring fundamental physics of magnetism and realizing spintronic applications with low power dissipation. Electric-field-controlled saturation magnetization, coercive force, T_c, and antiferromagnet−ferromagnet transitions have been the most extensively studied in ferromagnetic semiconductors and metallic ferromagnets (CrI_3, $Cr_2Ge_2Te_6$, (Ga,Mn)As, Fe_3GeTe_2).[6,9−13] In particular, the T_c of Fe_3GeTe_2 increases to room temperature via an additional ionic gate.[6] The pressure-induced antiferromagnetic-to-ferromagnetic transition is reported in bilayer CrI_3.[14,15] Moreover, the ferromagnetic or antiferromagnetic order of bilayer $CrBr_3$ can also be determined with a stacking structure via different interlayer magnetism.[16] The T_c of Mn_xGe_{1-x} nanomesh drastically increases, benefiting from the decreased mesh width, in which the quantum confinement effect in low-dimensionality Mn_xGe_{1-x} nanomesh can strongly enhance the exchange coupling.[17,18] Recent experiments have also revealed that a local puncture can induce a substantially enhanced magnetization.[19] Molecular beam epitaxy (MBE)-grown monolayer VSe_2 with a small crystal size generates room-temperature ferromagnetism, whereas its bulk counterpart is paramagnetic.[8]

The magnetic properties of bulk chromium(III) telluride (Cr_2Te_3) have been carefully studied; the chemical composition and crystal structure dominate the ferromagnetic properties (T_c is about 195 K).[20] The neutron diffraction revealed a ferromagnetic ordering process of bulk Cr_2Te_3 along the *c*-axis and discovered intrinsic contraction of the unit cell as the temperature decreases.[21,22] The average magnetic moment is only about 2.7 μ_B in this material, which is smaller than that for three unpaired electrons in the Cr^{3+} ion. Goodenough suggests that this decrease possibly originated from a spiral antiferromagnetic spin arrangement, and an alternative mechanism

Received: December 13, 2019
Revised: April 7, 2020
Published: April 27, 2020

https://dx.doi.org/10.1021/acs.nanolett.9b05128
Nano Lett. 2020, 20, 3130−3139

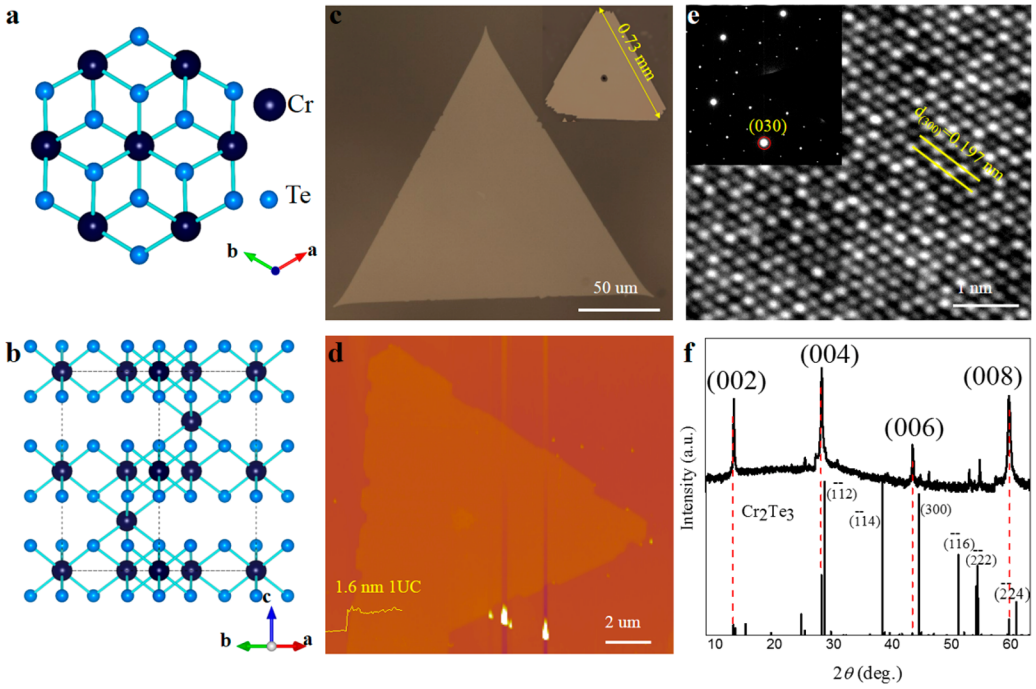

Figure 1. Morphology and structure of Cr_2Te_3. (a,b) Atomic structure (top and side views) of Cr_2Te_3. The 1 UC is 1.207 nm. (c) Optical micrograph images of CVD-grown Cr_2Te_3 show a large size of >190 μm. The inset shows the large-sized Cr_2Te_3 of >0.73 mm. (d) AFM image of 1 UC Cr_2Te_3 (1.6 nm). (e) HRTEM image indicates the (300) lattice constant at 0.197 nm. The SAED shows the hexagonal crystal structures of Cr_2Te_3 in the inset of (e). (f) XRD spectra of Cr_2Te_3 transferred to the SiO_2/Si substrate.

proposed by Andresen indicates that this phenomenon may account for the tilted moment.[21,23] 2D materials, with reduced dimensionality up to the atomically thin level, exhibit exceptional physical properties, such as the enhancement of critical temperature in 2H-TaS_2,[24,25] robust room-temperature ferroelectricity,[26,27] and enhanced charge-density-wave transition temperature.[28] However, as the dimension is reduced, the decrease of T_c is a universal trend in ferromagnetic semiconductors ($Cr_2Ge_2Te_6$ and CrI_3)[4,5] and metallic ferromagnets (Fe_3GeTe_2, Ni, Fe, Co, and Nb/Gd).[29−33]

In this work, we realize the synthesis of 1, 2, and 4 unit cell (UC) Cr_2Te_3 single-crystal and millimeter-scale single crystal via van der Waals epitaxy on a mica substrate. Interestingly, an anomalous thickness-dependent T_c is discovered where the thinner Cr_2Te_3 shows a higher T_c value. Moreover, with the reduced thickness up to 7.1 and 5.5 nm, the hall resistance (R_{xy}) exhibits an obvious hysteresis loop until the temperature increases to 280 K. The nonzero remanent Hall resistance (R_r) is still observed at 280 K, which provided unambiguous evidence for the existence of spontaneous magnetization at room temperature. More importantly, the T_c is enhanced strongly from 160 K in the thick flake (40.3 nm) to 280 K in the 4 UC Cr_2Te_3 (5.5 nm). When compared with its bulk counterpart, the Bragg peaks in 2D Cr_2Te_3 shows slight shift toward a higher degree than bulk, which indicates that the lattice parameter along the *c*-axis of 2D Cr_2Te_3 is smaller than that in the bulk. This result is consistent with our density functional theory (DFT) calculation and further confirms that the higher T_c observed in ultrathin Cr_2Te_3 (compared to bulk) probably originates from the decrease in lattice parameter that resulted from the reconstruction of Cr_2Te_3.

Result and Discussion. The millimeter-scale Cr_2Te_3 (over 0.93 mm) is prepared by atmospheric pressure chemical vapor deposition (APCVD) (Figure S1b; see Methods section). Also, Cr_2Te_3 that exhibits a large size (greater than 190 μm) and a thickness approximately 5.1 nm is grown using a similar technique (see Figure 1c and Figure S2c). The inset of Figure 1c shows the large-sized Cr_2Te_3 of more than 0.73 mm with a thickness of 19.5 nm. According to the theoretical model (Figure 1b), the size of the 1 UC is estimated to be 1.207 nm. Combining the height profile of an atomic force microscopy (AFM) measurement with the theoretical model, it can be inferred that the sample with the thicknesses of 1.6, 3.1, and 5.1 nm are 1, 2, and 4 UC, respectively (Figure 1d and Figure S2b,c). Note that the Cr_2Te_3 with the thickness of 1 UC is almost invisible via optical microscopy. The high-resolution transmission electron microscopy (HRTEM) images of Cr_2Te_3 are shown in Figure 1e. The distinct lattice constant with a spacing of 0.197 nm is observed, which matches exactly with the (300) plane of Cr_2Te_3 according to the PDF card (PDF#71-2245). Furthermore, the selected area electron diffraction (SAED) result indicates that the Cr_2Te_3 exhibits hexagonal crystal structures. The X-ray diffraction (XRD) pattern of Cr_2Te_3 (Figure 1f), which is transferred to the SiO_2/Si substrate, matches well with the standard PDF card (PDF# 71-2245). In addition, the XRD pattern only shows (00*X*) peaks, which suggests that the crystal surface is perpendicular to the *c*-axis. According to the HRTEM and SAED analysis [(*hk*0) plane], the distinct lattice and a set of diffraction spots demonstrate that the Cr_2Te_3 is one single domain in these planes, which shows the labels of the corresponding lattice indices in Figures S3 and S4. In addition, regular triangular characters (as shown in Figure S3a) and sharp XRD diffraction patterns [(00*l*) peaks] further verify the high crystallization quality of Cr_2Te_3 flakes. Furthermore, we select two Cr_2Te_3 flakes on a random basis, and then we confirm that the SAED patterns at the same triangular Cr_2Te_3 in different regions exhibit nearly identical crystallographic orientations (error

https://dx.doi.org/10.1021/acs.nanolett.9b05128
Nano Lett. 2020, 20, 3130−3139

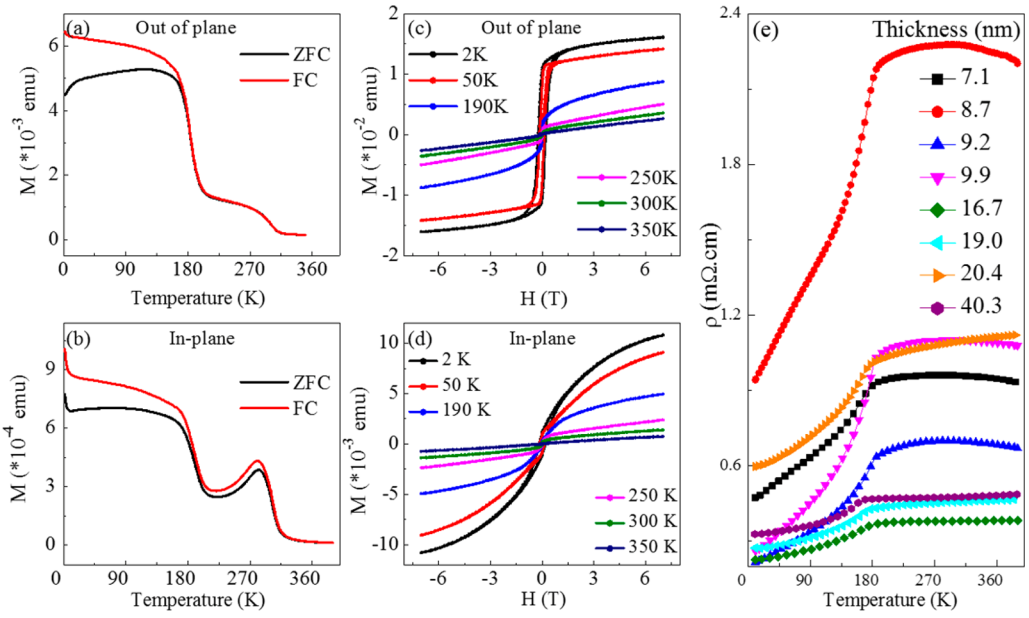

Figure 2. Magnetic properties and electrical transport measurements of Cr_2Te_3. (a,b) Temperature-dependent magnetic susceptibility measured on mica substrates with a field of 0.1 T for out-of-plane and in-plane. The ultrathin and thick Cr_2Te_3 are randomly distributed on the mica substrate. (c,d) Field-dependent magnetization on mica substrates at some specific temperature with applied field from −7 to +7 T for out-of-plane and in-plane, respectively. (e) Temperature-dependent electrical transport measurements of longitudinal resistance (R_{xx}) as thicknesses are varied.

within ±0.09°), as shown in Figures S3 and S4. Therefore, with combined regular triangular characters, sharp XRD, and diffraction patterns, we demonstrate that each triangular crystal has essentially one single domain in these planes. When the SAED patterns are captured, the instrument automatically corrects the brightness. Therefore, the SAED patterns obtained exhibit variations in the peak intensities at different positions. In addition, the wrinkle of Cr_2Te_3 also affects the peak intensities. Further, we selected five Cr_2Te_3 flakes on a random basis. A set of diffraction spots with hexagonal crystal structures demonstrates that all Cr_2Te_3 is the same crystal structure, as shown in Figures S5 and S6. The (300) lattice constant of all samples is about 0.197 nm. The XRD patterns show consistent (00l) peaks. Therefore, we demonstrate that the triangular Cr_2Te_3 is single crystal, and all Cr_2Te_3 exhibit the same crystalline phase. From the XRD and TEM analyses, it can be deduced that only a single phase is present. The binding energies of two elements (Cr and Te) are very close; hence, the stoichiometric relation cannot be achieved via X-ray photoelectron spectroscopy. We can estimate the chemical composition via transmission electron microscopy and energy-dispersive X-ray spectroscopy (TEM-EDX), and the stoichiometric ratio of Cr and Te is approximately 2:3.04. We identify the stoichiometric relation by comparing the structural characteristics between our sample and other Cr−Te compounds, then, we find that the PDF card (PDF# 71-2245) of Cr_2Te_3 has the greatest similarity with our sample's XRD pattern and TEM analysis. Further, the TEM mapping indicates the uniform distribution of Cr and Te elements throughout the whole crystal (Figure S7). There is no indication that the Cr or Te element is concentrated at the surface.

The magnetization measurements performed using the as-synthesized ultrathin and thick Cr_2Te_3 are shown in Figure 2a−d, where ultrathin and thick flakes are randomly distributed on the mica substrate. The magnetic susceptibility behavior for both in-plane and out-of-plane is similar, where they show two magnetic phase transitions and have similar temperature values in every transition, as shown in Figure 2a,b and Figure S10a,b. In the case of the out-of-plane direction, a room-temperature magnetic phase transition appears at about $T_{c\text{-thin}}$ = 300 K ($T'_{c\text{-thin}}$ = 301 K for in-plane). Also, decreasing the temperature to about $T_{c\text{-thick}}$ = 185 K ($T'_{c\text{-thick}}$ = 189 K for in-plane) abruptly increases the magnetic susceptibility. Furthermore, small hysteresis is observed at 190, 250, and 300 K when the corresponding temperature is below $T_{c\text{-thin}}$ and above $T_{c\text{-thick}}$, as shown in Figure 2c and Figure S8a,b. From the $\chi-T$ and $M-H$ data, Cr_2Te_3 shows a ferromagnetic-like behavior. Below $T_{c\text{-thick}}$, a strong magnetization occurs with a near saturation value of about 0.015 emu at 2 K and 7 T, and there is a magnetization value of 0.0086 emu at 7 T until 190 K. However, when this temperature exceeds about 300 K, Cr_2Te_3 has a paramagnetic order with a linear field-dependent magnetization. However, in the in-plane direction, although the magnetic properties are similar to those of the out-of-plane direction, there are still have some differences. First, the value of magnetic susceptibility within the *ab* plane (in-plane) is near 7 times lower than that along the *c*-axis (out-of-plane) direction with the temperature range from 2 to 350 K. Additionally, within the temperature range of 280−220 K, the susceptibility within the *ab* plane decreased with decreasing temperature, which is different from that along the *c*-axis direction: the susceptibility is monotonically increased with decreasing temperature. On the other hand, below 1 T, the moment along the *c*-axis increases sharper than that in the *ab* plane; as the magnetic susceptibility further increases, the moment along the *c*-axis becomes nearly saturated, but that in the *ab* plane still rapidly increases. According to those phenomena, Cr_2Te_3 film shows strong magnetocrystalline anisotropy, and the easy magnetization axis of the magnetic phase transition near 300 K is probably along the [001] (*c*-axis) direction, which means that below $T_{c\text{-thin}}$ (or $T'_{c\text{-thin}}$) the magnetic moment will turn to the [001] direction gradually. Therefore, along the *c*-axis direction, the susceptibility

https://dx.doi.org/10.1021/acs.nanolett.9b05128
Nano Lett. 2020, 20, 3130−3139

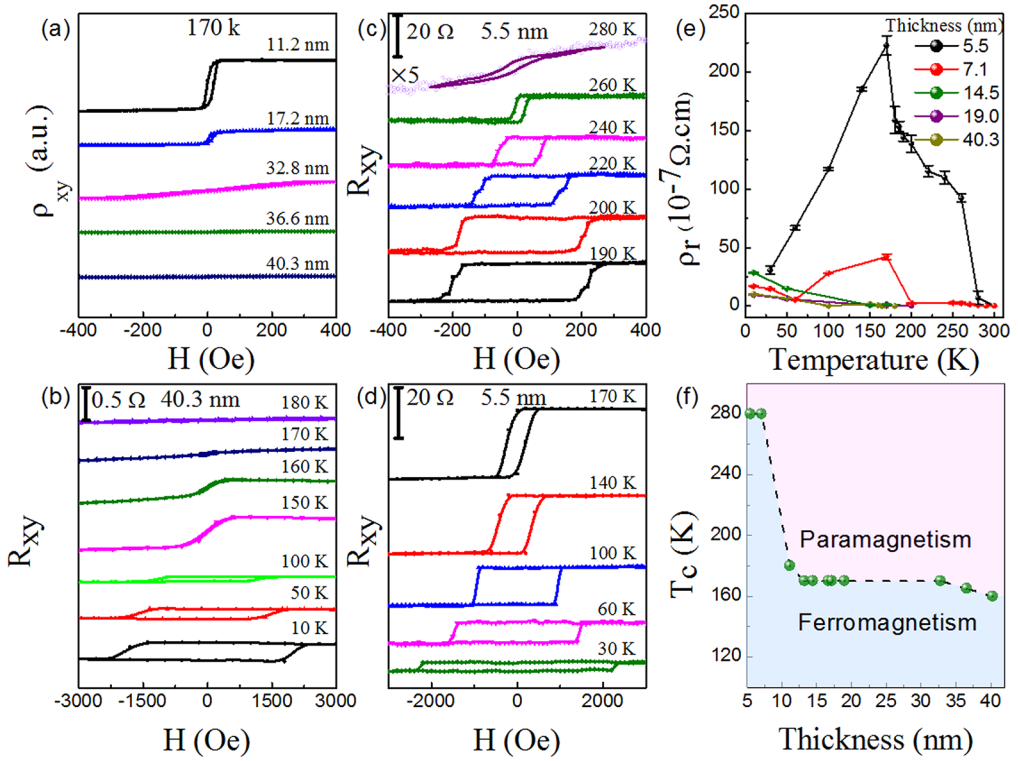

Figure 3. Magnetic transport measurements. (a) External magnetic field (H) dependence Hall electrical resistivity ρ_{xy} as thicknesses are varied. (b–d) H-dependent R_{xy} with thicknesses of 40.3 and 5.5 nm at different temperature; the purple solid line is a guide for the eyes in (c). There is still hysteresis at 280 K, with a thickness of 5.5 nm, which provided unambiguous evidence for the existence of spontaneous magnetization at room temperature. (e) T-dependent remanent Hall electrical resistivity (ρ_r) for different thicknesses. (f) Phase diagram of Cr_2Te_3. We extract remanent Hall resistance (R_r) at zero field, which can be used to estimate the T_c. The ferromagnetism phase transition temperature increases when the thickness of Cr_2Te_3 is decreased and is enhanced strongly when the thickness is less than 7.1 nm.

continuously increases with decreasing temperature, but within the *ab* plane, the susceptibility increases at first instantly and decreases gradually, which is also consistent with the $\chi-T$ data. In order to exclude the mechanism of the room-temperature magnetic transition that might originate from the substrate or the interaction between the substrate and the sample, different samples with mica and SiO_2 substrates were measured. The field-dependent magnetization is shown in Figure S8a–c, which shows the ferromagnetic-like behavior. As displayed in Figure 2a,b, the magnetic susceptibilities show the same order of magnitude in two transitions for both in-plane and out-of-plane. The weight of Cr_2Te_3 grown by the CVD method, including the mica substrates, was about 0.92 mg. Hence, the saturation moment of Cr_2Te_3 can be roughly estimated to be about 14.0 and 2.3 emu/g at 50 and 300 K, respectively, and with 3 T (out-of-plane). This result is similar to the reported saturation moment of $Cr_{0.62}Te$, which is about 40 emu/g at 5 K.[34] In MoS_2 and graphite,[35,36] the saturation moment is about 10^{-3} to 10^{-2} emu/g when the temperature is lower than the magnetic order temperature, T_c, which is 3 or 2 orders of magnitude smaller than that in Cr_2Te_3 below $T_{c\text{-thin}}$. On the other hand, the strongly temperature-dependent coercivity also indicates the defect-induced ferromagnetism is not dominated.[36,37]

The electrical transport measurements of longitudinal resistance (R_{xx}) were performed from 390 to 10 K. The electrical resistivity, which is defined as $\rho = R_{xx}S/L$ (where S is the cross-sectional area and L represents the longitudinal length of devices) for the thick Cr_2Te_3 with a thickness of 40.3 nm, decreases monotonously with decreasing temperature in the whole temperature range (Figure 2e). Furthermore, the Cr_2Te_3 exhibits obvious metallic behavior when the thickness is reduced from 40.3 to 16.7 nm. The kinks were observed around 170 K, matching the ferromagnetism phase transition temperature (T_c). Then, magnetic transport measurements were carried out for further extracting T_c via anomalous Hall effect (AHE). The AHE usually appears in ferromagnetic materials in which the time-reversal symmetry is broken.[38] Basically, the Hall resistance (R_{xy}) can be ascribed to the anomalous Hall resistance (R_{AH}) and the normal Hall resistance (R_{NH}). Hence, $R_{xy} = R_0H_z + R_sM_z$, where R_0 and R_S are coefficients, and H_z and M_z are perpendicular field and magnetization, respectively.[6,38] The anomalous Hall resistance originates from spontaneous magnetization. Also, the normal Hall resistance has a proportional relationship with H_z, derived from the Lorentz force. The spontaneous magnetization arouses a nonzero Hall response at zero magnetic field. Hence, we extract remanent Hall resistance (R_r) at zero field, which can be used to estimate the T_c. The extracted thickness-dependent Hall electrical resistivity, $\rho_{xy} = R_{xy}S/L_{xy}$, is shown in Figure 3a. The thinner Cr_2Te_3, including 11.2 and 17.2 nm thicknesses, exhibit more obvious anomalous Hall effect compared to that with the thick Cr_2Te_3 (32.8, 36.6, and 40.3 nm). Furthermore, we can estimate the T_c according to nonzero Hall response at zero magnetic field. Interestingly, an anomalous thickness-dependent T_c is discovered. As the dimensions of the ferromagnet are decreased, a strong decrease in T_c is quite common because of the domination of interlayer magnetic coupling.[4,29,30] In our specific case, the thinner Cr_2Te_3 shows a higher ferromagnetism phase transition

https://dx.doi.org/10.1021/acs.nanolett.9b05128
Nano Lett. 2020, 20, 3130–3139

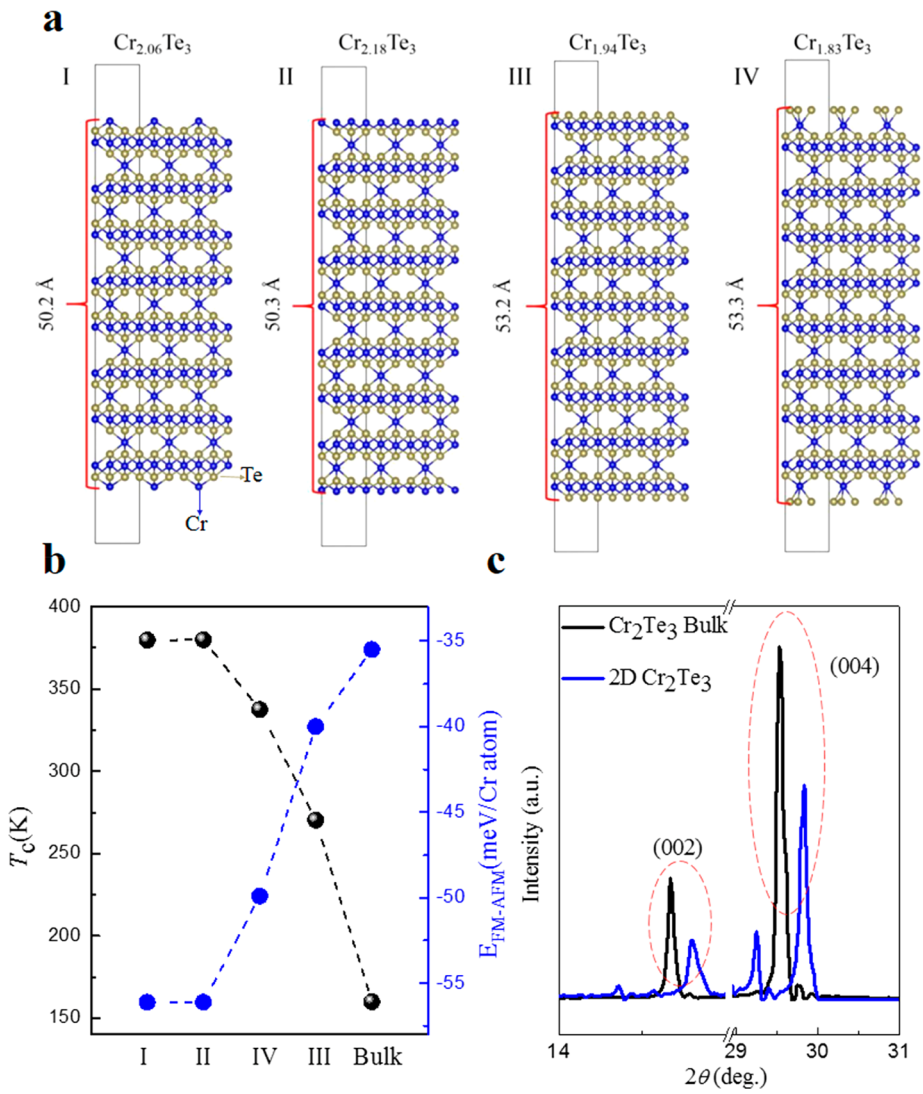

Figure 4. Theoretical model for anomalous T_c. (a) Four kinds of structures with different exposed atoms at the surface. (b) Exposed atoms dependent on Curie temperature and the energy difference between ferromagnetic state and antiferromagnetic state E_{FM-AFM}. (c) XRD spectra of bulk and 2D Cr_2Te_3 on a mica substrate. The (002) and (004) Bragg peaks of 2D Cr_2Te_3 shift to higher degree than bulk, which indicates that the lattice parameter of 2D Cr_2Te_3 is smaller than that of bulk.

temperature. In our condition, the magnetism of Cr_2Te_3 behaves as the bulk when the thickness is above 40 nm, according to the nonzero Hall response at zero magnetic field. The T_c, which is extracted via nonzero Hall response at 0 (Oe), is about 180, 170, 165, and 160 K for corresponding thickness of 11.2, 17.2, 36.6, and 40.3 nm, respectively (see Figure 3a,b and Figure S12b,d,e). The T_c of Cr_2Te_3 decreases from 180 to 160 K when the thickness increases from the 2D limit (approximately 11.2 nm) to bulk (approximately 40.3 nm). In addition, the Hall resistance exhibits classical rectangular hysteresis loops below 100 K when a perpendicular magnetic field is applied using a Cr_2Te_3 sample with a thickness of 40.3 nm (Figure 3b). When the temperature increases to 160 K, we also observe warp and remanent Hall resistance at zero magnetic field.

With a reduced thickness up to 5.5 nm, the R_{xy} exhibits obvious hysteresis loops until the temperature is increased to 280 K (Figure 3c,d). The nonzero R_r is still observed at 280 K, which provides unambiguous evidence for the existence of spontaneous magnetization at room temperature. Significantly, the T_c enhances strongly from 160 K in the thick flake (40.3 nm) to 280 K in the 4 UC Cr_2Te_3 (5.5 nm). In addition, this result exhibits good repeatability. As shown in Figure S14, the thicker 7.1 nm Cr_2Te_3 also exhibits room-temperature ferromagnetism with nonzero R_r at 280 K. The strongly temperature-dependent coercivity via an anomalous Hall effect further demonstrates that the defect-induced ferromagnetism is not responsible for room-temperature ferromagnetism.[18,19] Figure 3e shows the T-dependent remanent Hall electrical resistivity (ρ_r) for different thicknesses. Accordingly, the thinner Cr_2Te_3 exhibit more obvious remanent Hall electrical resistivity compared to that of the thick Cr_2Te_3. For the thinner samples, the remanent Hall resistivity decreases with the temperature when it is below 170 K. We think that it probably originates from the reorientation of a magnetic moment, which is kept away from the [001] direction as the temperature is decreased to less than 170 K. We extract remanent Hall resistance (R_r) at zero field. The remanent Hall resistance (R_r) can be ascribed to $R_r = R_s M_z$, with coefficients R_s and magnetization M_z. Due to the reorientation of the

https://dx.doi.org/10.1021/acs.nanolett.9b05128
Nano Lett. 2020, 20, 3130−3139

Table 1. Detailed Calculating Data, Including the Calculated Energy of Ferromagnetic State E_{FM} and Antiferromagnetic State E_{AFM}, Energy Difference between Ferromagnetic State and Antiferromagnetic State $E_{FM\text{-}AFM}$, Formation Energy E_{form}, and Curie Temperature T_c

structure	thickness (Å)	E_{FM} (eV)	E_{AFM} (eV)	$E_{FM\text{-}AFM}$ (meV/Cr atom)	E_{form} (eV/atom)	T_c (K)
I	50.2	−435.675	−433.822	−56.1	−0.667	379.7
II	50.3	−447.743	−445.778	−56.1	−0.628	379.8
III	53.2	−474.266	−472.867	−40.0	−0.672	270.3
IV	53.3	−454.535	−452.889	−49.9	−0.621	337.5
bulk	∞	−107.482	−107.198	−35.5	−0.691	160.0

magnetic moment, the remanent moment along the [001] direction will also decrease, which will result in the decrease of the remanent Hall resistivity. Based on the thickness-dependent T_c displayed in Figure 3f, we noticed that the ferromagnetism phase transition temperature of Cr_2Te_3 increases when its thickness decreases, and it is strongly enhanced when the thickness is less than 7.1 nm. The 4 UC Cr_2Te_3 (5.5 nm) shows obvious hysteresis loops at low temperature and a strongly temperature-dependent coercive field, as shown in Figure S12f.

To understand the underlying physical mechanisms of anomalous thickness-dependent T_c, we constructed four models with different surfaces, named I, II, III, and IV. The thicknesses in these models are approximately 5 nm, as shown in Figure 4a. In order to determine the ground state of these four models, we calculated the total energy of their ferromagnetic and antiferromagnetic states (see Table 1). We find the four models and the bulk model present ferromagnetic ground states, no matter which kind of atom is exposed to the surface. In other words, the ferromagnetic ground states of the material are independent of the atomic configuration at the surface. However, the energy difference between the ferromagnetic state and the antiferromagnetic state is different for the four models, which suggests different T_c could exist. The calculated values of T_c are shown in Figure 4b and Table 1. The theoretical results are larger than that measured in the experiment, which can be attributed to the actual complexity and accuracy of theoretical calculations.[39,40] Thus, we introduce a heuristic scaling factor of 0.583 to calibrate the theoretical T_c values, and the T_c values reduce to 379.7, 379.8, 270.3, 337.5, and 160.0 K for models I, II, III, IV, and bulk, respectively. Interestingly, the T_c of ultrathin Cr_2Te_3 is higher than the bulk one, which is consistent with the experimental results.

The mechanism of room-temperature ferromagnetism in 2D Cr_2Te_3 is an open question. The possible origin may be attributed to a doping mechanism or reconstruction of 2D Cr_2Te_3. The exposed atoms on the surface can result in slightly different surface stoichiometries, which could be a mere doping effect. When Cr_2Te_3 approaches the 2D limit, the mere doping effect can tune ferromagnetism, but the mere doping effect is negligible for bulk Cr_2Te_3. This is consistent with the seminal paper by Haraldsen,[20] in which the T_c of the Cr−Te system exhibits an extremely high sensitivity to Te element content. According to our theoretical calculation, the Te element content will be changed owing to the exposed atoms on the surface when Cr_2Te_3 approaches the 2D limit. However, the change of Te element content with different exposed atoms on the bulk Cr_2Te_3 is negligible. When Cr_2Te_3 approaches the 2D limit, the change of Te element content may result in the change of T_c.[21] In fact, the change of Te element content can result in the change of T_c indeed, with a thickness similar to that in our theoretical model. However, we are unable to access precise element analysis for identifying the stoichiometric compound of each thickness at the present stage. Significantly, the T_c of all samples obeys the law that the T_c of the Cr_2Te_3 increases when the thickness decreases from 40.3 to 5.5 nm. An anomalous thickness-dependent T_c is discovered. The thinner Cr_2Te_3 shows higher T_c via analysis of all samples. Therefore, the enhancement of T_c is related to the thickness. The entire structure was compressed via theoretical calculations, and the biggest change of nearest Cr atoms along the *c*-axis appears on the surface. The distances of surface nearest Cr atoms along the *c*-axis are 3.007, 3.173, 3.159, and 3.086 Å in models I, II, III, and IV, respectively. The distances of center nearest Cr atoms along the *c*-axis are 3.215, 3.216, 3.219, and 3.214 Å in models I, II, III, and IV, respectively. The distance of nearest Cr atoms along the *c*-axis is 3.220 Å in the bulk. The weak interaction between substrates and Cr_2Te_3 in van der Waals epitaxy does not result in a change of lattice parameters. However, owing to the nonlayered character of Cr_2Te_3, dangling bonds of nonlayered Cr_2Te_3 possess high energy, which result in the reconstruction and change of lattice parameters. The distance of nearest atoms (Cr) in ultrathin Cr_2Te_3 becomes nearer owing to reconstruction, especially surface reconstruction.

According to the Heisenberg's model

$$E = -\sum_{i,j} J_{ij} S_i S_j \quad (i \neq j)$$

where S_i and S_j represent the spin of the ions in i and j sites, respectively. J_{ij} is the exchange integral between the different ions i and j, which can be written as follows:

$$J_{ij} = \int \phi_i^*(r_i)\phi_j^*(r_j)V(r_{ij})\phi_i(r_i)\phi_j(r_j)\mathrm{d}r_i\mathrm{d}r_j, \quad V(r_{ij}) = \frac{Ke^2}{4\pi r_{ij}}$$

where r_{ij} is the distance between atoms i and j and $V(r_{ij})$ is the Coulomb interaction potential.

With the exchange integral value of the J_{ij} increasing with the distance r_{ij} decreasing, considering the mean-field approximation, the Curie temperature T_c can be estimated by solving the following equation:[41,42]

$$\langle S_i^Z \rangle = \frac{S_i(S_i+1)}{3k_BT} \sum_j J_{ij} \langle S_j^Z \rangle$$

Here, k_B is the Bolzmann constant. The T_c can be obtained from the largest eigenvalue of the matrix $\Theta_{ij} = S_i(S_i + 1)J_{ij}/3k_B$. In this case, the T_c will increase with the increasing J_{ij}. Hence, the Curie temperature of ultrathin Cr_2Te_3 will be higher than that of the ideal bulk Cr_2Te_3. The XRD pattern only shows (00*X*) peaks, which suggests the crystal surface is perpendicular to the *c*-axis. From Figure 4c, we can see that the (002) and (004) Bragg peaks of 2D Cr_2Te_3 shift to a higher degree

https://dx.doi.org/10.1021/acs.nanolett.9b05128
Nano Lett. 2020, 20, 3130−3139

than bulk, which indicates that the lattice parameter along the *c*-axis of 2D Cr_2Te_3 is smaller than that of the bulk. This experimental result is consistent with the DFT calculation result and confirms that the higher T_c of 2D Cr_2Te_3 (compared to that of the bulk) probably originates from the decrease of the lattice parameter that resulted from the reconstruction of 2D Cr_2Te_3. From the calculation of XRD data, the specific interplanar distances $d_{(001)}$ of 2D and bulk Cr_2Te_3 are 11.994 ± 0.005 and 12.109 ± 0.001 Å, respectively. The specific interplanar distance $d_{(001)}$ of 2D Cr_2Te_3 exhibits a value smaller than that of bulk Cr_2Te_3, and the difference between 2D and bulk Cr_2Te_3 is about 0.115 Å. According to the DFT calculation, the *d* values of 2D and bulk Cr_2Te_3 are 12.57 and 12.88 Å. The variation tendency is consistent with the XRD analysis, and the difference between 2D and bulk Cr_2Te_3 is about 0.310 Å, which is comparable to the results calculated by the XRD data. Based on those data, we speculate that the anomalous thickness dependence of T_c probably originates from the reconstruction, but we cannot rule out the doping mechanism. The (00l) peak of 2D and bulk Cr_2Te_3 synthesized by CVD exhibits similar positions and relative height with Cr_2Te_3 PDF card (PDF# 71-2245), so the synthesized Cr_2Te_3 probably has the same structure with the previous reports as shown by the PDF card. Because the weight of Cr_2Te_3 powder grown by CVD is not enough, it is hard to get the powder XRD pattern of 2D and bulk Cr_2Te_3 at the present stage.

In order to compare the stability of these structures, we also calculate the formation energy. The results show that model III ($Cr_{1.94}Te_3$) exhibits minimum formation energy, and the T_c increases strongly from 160.0 K in the bulk to 270.3 K, which is very close to our experimental result. This can be ascribed to a larger energy difference between the ferromagnetic state and the antiferromagnetic state. Therefore, we presume that the room-temperature ferromagnetism originates from the reconstruction which brings about a sharp increase in T_c.

Conclusion. In summary, we fabricated 1, 2, and 4 UC Cr_2Te_3 single crystals and revealed a room-temperature ferromagnetism in ultrathin Cr_2Te_3. An anomalous thickness-dependent T_c is also discovered. The newly observed T_c increases strongly from 160 K in the thick flake (40.3 nm) to 280 K in the 6 UC Cr_2Te_3 (7.1 nm). The magnetization measurements and robust Hall effect provide unambiguous evidence for the existence of spontaneous magnetization at room temperature. The large saturation moment and strongly temperature-dependent coercivity indicate that the room-temperature ferromagnetism is the intrinsic characteristic. The theoretical model indicates the reconstruction bring about anomalous thickness-dependent T_c. The dimension tuning method paves a way for investigating the fundamental studies in 2D ferromagnetism and designing new van der Waals spintronic architecture.

Methods. *Growth of Large-Sized Cr_2Te_3.* To obtain Cr_2Te_3, the atmospheric pressure chemical vapor deposition (APCVD) method was employed. In the typical synthesis, the tellurium powder (200 mesh, 99.999%) and chromium(III) chloride ($CrCl_3$ 98%) were used as precursor materials. Initially, the quartz tube was kept in a two-zone furnace. The Te was placed in the front zone at 550 °C, and the mixture of $CrCl_3$ and NaCl was placed behind at 850 °C. The mica substrate was then kept near the $CrCl_3$ powder. For the synthesis of this material, a constant flow rate of 150 sccm was maintained, and H_2 and Ar were used as the carrier gas.

Fabrication of Devices. Benefiting from the large size of Cr_2Te_3, the atomically flat Au electrodes with a thickness of 150 nm can be transferred to the Cr_2Te_3 via a probe. The probe adheres Au electrodes via a Ga−In alloy and then releases the Au electrodes on target flakes. The atomically flat Au electrodes were fabricated by thermal evaporation via a shadow mask on SiO_2/Si substrates. The poly(methyl methacrylate) (PMMA) was spin-coated on target substrates, which can contribute to tight contact between Au electrodes and flakes. The Au wires are in contact with Au electrodes with conductive silver adhesives. According to the HRTEM, XRD, and SAED analysis, we demonstrate that the regular triangular Cr_2Te_3 represents a single-crystal characteristic. When the transport measurements were executed, the Cr_2Te_3 with a regular triangle was used to fabricate the devices.

Characterizations. When the X-ray diffraction measurement was carried out, Cr_2Te_3 was transferred to the SiO_2/Si substrate from mica (mica showed a large number of XRD peaks). PMMA was spin-coated on Cr_2Te_3/mica substrates and used as the supporting film. Deionized water facilitates the separation of PMMA/Cr_2Te_3 and mica substrates. Significantly, the transfer of crystals can result in damage to the sample. Therefore, all electrical transport characterization of Cr_2Te_3 was carried out on mica substrates. The microstructure morphology of the as-synthesized material was examined with an optical microscope (Leica). The thickness was measured by atomic force microscopy (Asylum Research MFP-3D Infinity). The X-ray diffractometer (D8 Focus, Bruker) was used to identify the crystal structure. Transmission electron microscopy (Tecnai G2 F20 FEI) was used for achieving lattice constant and element distribution.

Magnetic Property Measurements. The magnetic susceptibility and magnetization measurements were carried out using a superconducting quantum interference device magnetometer (Quantum Design, MPMS-VSM). Two modes (zero field cooling and field cooling) were used to measure the magnetic susceptibility at 0.1 T. In-plane, magnetic susceptibility studies were carried out within the temperature range from 2 to 390 K, and the magnetization was measured at temperatures of 2, 50, 190, 250, 300, and 350 K by a magnetic field from −7 to +7 T. Out-of-plane, the temperature range of magnetic susceptibility was 2−350 K, and the magnetization was measured at some selected temperatures (2, 50, 190, 250, 300, and 350 K) by the magnetic field from −7 to +7 T.

Electrical and Magnetic Transport Measurements. The resistivity was collected by a pulse relaxation method on a physical property measurement system calorimeter (Quantum Design, PPMS-9T) varying from 390 to 10 K for different samples with varied thickness. The Hall electrical resistivity (ρ_{xy}) was measured by a physical property measurement system calorimeter (Quantum Design, PPMS-9T) at some selected temperatures and with varying external magnetic fields (*H*) from −5000 to +5000 Oe or −500 to +500 Oe. The constant current of 100 μA was carried out in those experiments.

Calculation Methods for Anomalous Thickness-Dependent T_c. Here, in order to verify our experimental results and to analyze the physical mechanism, we carried out a theoretical simulation using the VASP (Vienna ab initio simulation) package based on density functional theory.[43,44] The exchange correlation potential is described with the Perdew−Burke−Ernzerhof (PBE) of the generalized gradient approximation (GGA).[45] To take into account the correlation effects of Cr 3d

https://dx.doi.org/10.1021/acs.nanolett.9b05128
Nano Lett. 2020, 20, 3130−3139

electrons, the GGA+U method is adopted,[46] and the values of the on-site Coulomb interaction U and exchange interaction J are set to be 3.0 and 0.9 eV, respectively.[47] The electron−ion potential is modeled with the projector-augmented wave (PAW) potential.[44] The kinetic energy cutoff of the plane wave is set to be 230 eV for the plane wave expansion. The Brillouin zone (BZ) integration is carried out using 3 × 3 × 1 Monkhorst−Pack k-point meshes for geometry optimization of the system.[48] The geometry structures are relaxed until the force on each atom is less than 0.01 eV/Å and the total energy convergence criteria is chosen as 10^{-5} eV.

To determine the energetically stable configuration, we stimulate the formation energy using the following formula:

$$E_{\text{form}} = (E_{\text{total}} - n_i\mu_i - n_j\mu_j)/N$$

where E_{total} is the total energy of the structure, n_i and n_j represent the number of Te and Cr atoms, respectively, μ_i and μ_j are the chemical potential of Te and Cr atoms, respectively, and N is the total number of atoms.

Based on the mean-field theory, the Curie temperature is calculated by the expression[49]

$$\gamma k_B T_c/2 = E_{\text{AFM}} - E_{\text{FM}}$$

where γ and k_B are the dimension of the system and the Boltzmann constant,[50] respectively.

■ ASSOCIATED CONTENT

Supporting Information

The Supporting Information is available free of charge at https://pubs.acs.org/doi/10.1021/acs.nanolett.9b05128.

Optical micrographs of CVD-grown Cr_2Te_3; AFM images and height profile of CVD-grown Cr_2Te_3; SAED patterns at the same triangular Cr_2Te_3 in different regions; SAED patterns at different triangular Cr_2Te_3; distribution of Cr and Te elements via TEM-EDX; field-dependent magnetization at different substrates; temperature dependence of differential magnetic susceptibility; electrical transport measurements of longitudinal resistance (R_{xx}); H-dependent R_{xy} with different thickness and temperature; AFM images and height profile of the devices; chemical composition analysis of TEM-EDX; band structure of the bulk Cr_2Te_3; bond valence sum calculation results; magnetic properties of Cr_2Te_3; mechanism of magnetic transition (PDF)

■ AUTHOR INFORMATION

Corresponding Authors

Youwen Long − *Beijing National Laboratory for Condensed Matter Physics, Institute of Physics, University of Chinese Academy of Sciences, Beijing 100049, China; Songshan Lake Materials Laboratory, Dongguan, Guangdong 523808, China;* orcid.org/0000-0002-8587-7818; Email: ywlong@iphy.ac.cn

Jun He − *School of Physics and Technology, Wuhan University, Wuhan 430072, China;* orcid.org/0000-0002-2355-7579; Email: hej@nanoctr.cn

Authors

Yao Wen − *School of Physics and Technology, Wuhan University, Wuhan 430072, China*

Zhehong Liu − *Beijing National Laboratory for Condensed Matter Physics, Institute of Physics, University of Chinese Academy of Sciences, Beijing 100049, China*

Yu Zhang − *School of Physics and Technology, Wuhan University, Wuhan 430072, China*

Congxin Xia − *Department of Physics, Henan Normal University, Xinxiang 453007, China;* orcid.org/0000-0003-1915-4264

Baoxing Zhai − *Department of Physics, Henan Normal University, Xinxiang 453007, China*

Xinhui Zhang − *State Key Laboratory of Superlattices and Microstructures, Institute of Semiconductors, University of Chinese Academy of Sciences, Beijing 100049, China;* orcid.org/0000-0003-0059-6599

Guihao Zhai − *State Key Laboratory of Superlattices and Microstructures, Institute of Semiconductors, University of Chinese Academy of Sciences, Beijing 100049, China*

Chao Shen − *State Key Laboratory of Superlattices and Microstructures, Institute of Semiconductors, University of Chinese Academy of Sciences, Beijing 100049, China;* orcid.org/0000-0002-3664-4874

Peng He − *CAS Center for Excellence in Nanoscience, National Center for Nanoscience and Technology, University of Chinese Academy of Sciences, Beijing 100049, China*

Ruiqing Cheng − *CAS Center for Excellence in Nanoscience, National Center for Nanoscience and Technology, University of Chinese Academy of Sciences, Beijing 100049, China;* orcid.org/0000-0002-3618-4759

Lei Yin − *CAS Center for Excellence in Nanoscience, National Center for Nanoscience and Technology, University of Chinese Academy of Sciences, Beijing 100049, China*

Yuyu Yao − *CAS Center for Excellence in Nanoscience, National Center for Nanoscience and Technology, University of Chinese Academy of Sciences, Beijing 100049, China*

Marshet Getaye Sendeku − *CAS Center for Excellence in Nanoscience, National Center for Nanoscience and Technology, University of Chinese Academy of Sciences, Beijing 100049, China*

Zhenxing Wang − *CAS Center for Excellence in Nanoscience, National Center for Nanoscience and Technology, University of Chinese Academy of Sciences, Beijing 100049, China*

Xubing Ye − *Beijing National Laboratory for Condensed Matter Physics, Institute of Physics, University of Chinese Academy of Sciences, Beijing 100049, China*

Chuansheng Liu − *School of Physics and Technology, Wuhan University, Wuhan 430072, China*

Chao Jiang − *CAS Center for Excellence in Nanoscience, National Center for Nanoscience and Technology, University of Chinese Academy of Sciences, Beijing 100049, China;* orcid.org/0000-0001-7889-0291

Chongxin Shan − *Henan Key Laboratory of Diamond Optoelectronic Materials and Devices, School of Physics and Engineering, Zhengzhou University, Zhengzhou 450052, China*

Complete contact information is available at: https://pubs.acs.org/10.1021/acs.nanolett.9b05128

Author Contributions

Y.W. and Z.L. contributed equally to this work. Y.W. and J.H. conceived the projects. Y.W. carried out the synthesis, characterization, and fabrication of the devices. Y.W. and Z.L. performed electric and magnetization measurements. C.X. and B.Z. carried out the DFT calculation. Y.W., Z.L., Y.L., and

https://dx.doi.org/10.1021/acs.nanolett.9b05128
Nano Lett. 2020, 20, 3130−3139

J.H. discussed and analyzed the results. Y.W., Z.L., Y.L., and J.H. wrote the manuscript. Y.L. and J.H. supervised the project.

Notes

The authors declare no competing financial interest.

■ ACKNOWLEDGMENTS

This work was supported by National Key R&D Program of China (Nos. 2018YFA0703700, 2016YFA0200700, 2018YFE0103200, and 2018YFA0305700), National Natural Science Foundation of China (Nos. 91964203, 61851403, 61625401, 11674072, 11934017, 11921004, 51772324, 11574378, and 11874128), and CAS projects (Grant Nos. QYZDB-SSW-SLH013, XDB30000000, GJHZ1773, and XDB07030300). The authors also gratefully acknowledge the support of Youth Innovation Promotion Association CAS.

■ REFERENCES

(1) Mermin, N. D.; Wagner, H. Absence of ferromagnetism or antiferromagnetism in one- or two-dimensional isotropic Heisenberg models. *Phys. Rev. Lett.* **1966**, *17*, 1133−1136.
(2) Magda, G. Z.; Jin, X.; Hagymási, I.; Vancsó, P.; Osváth, Z.; Nemes-Incze, P.; Hwang, C.; Biró, L. P.; Tapasztó, L. Room-temperature magnetic order on zigzag edges of narrow graphene nanoribbons. *Nature* **2014**, *514*, 608−611.
(3) Yazyev, O. V. Emergence of magnetism in graphene materials and nanostructures. *Rep. Prog. Phys.* **2010**, *73*, 056501.
(4) Gong, C.; Li, L.; Li, Z.; Ji, H.; Stern, A.; Xia, Y.; Cao, T.; Bao, W.; Wang, C.; Wang, Y.; Qiu, Z. Q.; Cava, R. J.; Louie, S. G.; Xia, J.; Zhang, X. Discovery of intrinsic ferromagnetism in two-dimensional van der Waals crystals. *Nature* **2017**, *546*, 265.
(5) Huang, B.; Clark, G.; Navarro-Moratalla, E.; Klein, D. R.; Cheng, R.; Seyler, K. L.; Zhong, D.; Schmidgall, E.; McGuire, M. A.; Cobden, D. H.; Yao, W.; Xiao, D.; Jarillo-Herrero, P.; Xu, X. Layer-dependent ferromagnetism in a van der Waals crystal down to the monolayer limit. *Nature* **2017**, *546*, 270.
(6) Deng, Y.; Yu, Y.; Song, Y.; Zhang, J.; Wang, N. Z.; Sun, Z.; Yi, Y.; Wu, Y. Z.; Wu, S.; Zhu, J.; Wang, J.; Chen, X. H.; Zhang, Y. Gate-tunable room-temperature ferromagnetism in two-dimensional Fe_3GeTe_2. *Nature* **2018**, *563*, 94−99.
(7) Fei, Z.; Huang, B.; Malinowski, P.; Wang, W.; Song, T.; Sanchez, J.; Yao, W.; Xiao, D.; Zhu, X.; May, A. F.; Wu, W.; Cobden, D. H.; Chu, J.-H.; Xu, X. Two-dimensional itinerant ferromagnetism in atomically thin Fe_3GeTe_2. *Nat. Mater.* **2018**, *17*, 778−782.
(8) Bonilla, M.; Kolekar, S.; Ma, Y.; Diaz, H. C.; Kalappattil, V.; Das, R.; Eggers, T.; Gutierrez, H. R.; Phan, M.-H.; Batzill, M. Strong room-temperature ferromagnetism in VSe_2 monolayers on van der Waals substrates. *Nat. Nanotechnol.* **2018**, *13*, 289−293.
(9) Jiang, S.; Shan, J.; Mak, K. F. Electric-field switching of two-dimensional van der Waals magnets. *Nat. Mater.* **2018**, *17*, 406−410.
(10) Jiang, S.; Li, L.; Wang, Z.; Mak, K. F.; Shan, J. Controlling magnetism in 2D CrI_3 by electrostatic doping. *Nat. Nanotechnol.* **2018**, *13*, 549−553.
(11) Huang, B.; Clark, G.; Klein, D. R.; MacNeill, D.; Navarro-Moratalla, E.; Seyler, K. L.; Wilson, N.; McGuire, M. A.; Cobden, D. H.; Xiao, D.; Yao, W.; Jarillo-Herrero, P.; Xu, X. Electrical control of 2D magnetism in bilayer CrI_3. *Nat. Nanotechnol.* **2018**, *13*, 544−548.
(12) Wang, Z.; Zhang, T.; Ding, M.; Dong, B.; Li, Y.; Chen, M.; Li, X.; Huang, J.; Wang, H.; Zhao, X.; Li, Y.; Li, D.; Jia, C.; Sun, L.; Guo, H.; Ye, Y.; Sun, D.; Chen, Y.; Yang, T.; Zhang, J.; Ono, S.; Han, Z.; Zhang, Z. Electric-field control of magnetism in a few-layered van der Waals ferromagnetic semiconductor. *Nat. Nanotechnol.* **2018**, *13*, 554−559.
(13) Matsukura, F.; Tokura, Y.; Ohno, H. Control of magnetism by electric fields. *Nat. Nanotechnol.* **2015**, *10*, 209−220.
(14) Song, T.; Fei, Z.; Yankowitz, M.; Lin, Z.; Jiang, Q.; Hwangbo, K.; Zhang, Q.; Sun, B.; Taniguchi, T.; Watanabe, K.; McGuire, M. A.; Graf, D.; Cao, T.; Chu, J.-H.; Cobden, D. H.; Dean, C. R.; Xiao, D.; Xu, X. Switching 2D magnetic states via pressure tuning of layer stacking. *Nat. Mater.* **2019**, *18*, 1298−1302.
(15) Li, T.; Jiang, S.; Sivadas, N.; Wang, Z.; Xu, Y.; Weber, D.; Goldberger, J. E.; Watanabe, K.; Taniguchi, T.; Fennie, C. J.; Fai Mak, K.; Shan, J. Pressure-controlled interlayer magnetism in atomically thin CrI_3. *Nat. Mater.* **2019**, *18*, 1303−1308.
(16) Chen, W.; Sun, Z.; Wang, Z.; Gu, L.; Xu, X.; Wu, S.; Gao, C. Direct observation of van der Waals stacking−dependent interlayer magnetism. *Science* **2019**, *366*, 983−987.
(17) Nie, T.; Tang, J.; Kou, X.; Gen, Y.; Lee, S.; Zhu, X.; He, Q.; Chang, L.-T.; Murata, K.; Fan, Y.; Wang, K. L. Enhancing electric-field control of ferromagnetism through nanoscale engineering of high-T_c Mn_xGe_{1-x} nanomesh. *Nat. Commun.* **2016**, *7*, 12866.
(18) Xiu, F.; Wang, Y.; Kim, J.; Hong, A.; Tang, J.; Jacob, A. P.; Zou, J.; Wang, K. L. Electric-field-controlled ferromagnetism in high-Curie-temperature $Mn_{0.05}Ge_{0.95}$ quantum dots. *Nat. Mater.* **2010**, *9*, 337−344.
(19) Thiel, L.; Wang, Z.; Tschudin, M. A.; Rohner, D.; Gutiérrez-Lezama, I.; Ubrig, N.; Gibertini, M.; Giannini, E.; Morpurgo, A. F.; Maletinsky, P. Probing magnetism in 2D materials at the nanoscale with single-spin microscopy. *Science* **2019**, *364*, 973−976.
(20) Haraldsen, H.; Neuber, A. A. Magnetochemische untersuchungen. XXVII. magnetische und röntgenographische untersuchungen am system chrom−tellur. *Z. Anorg. Allg. Chem.* **1937**, *234*, 353−371.
(21) Andresen, A. F.; Rasmussen, S. E.; Hirvisalo, E. L.; Munch-Petersen, J.; Munch-Petersen, J. A neutron diffraction investigation of Cr_2Te_3 and Cr_5Te_6. *Acta Chem. Scand.* **1963**, *17*, 1335−1342.
(22) Hamasaki, T.; Hashimoto, T.; Yamaguchi, Y.; Watanabe, H. Neutron diffraction study of Cr_2Te_3 single crystal. *Solid State Commun.* **1975**, *16*, 895−897.
(23) Goodenough, J. B. Types of Magnetic Order. In *Magnetism and the Chemical Bond*; Cotton, F. A., Ed.; Interscience Publishers Inc.: New York, 1963; Vol. *I*, pp 75−156.
(24) Navarro-Moratalla, E.; Island, J. O.; Mañas-Valero, S.; Pinilla-Cienfuegos, E.; Castellanos-Gomez, A.; Quereda, J.; Rubio-Bollinger, G.; Chirolli, L.; Silva-Guillén, J. A.; Agraït, N.; Steele, G. A.; Guinea, F.; van der Zant, H. S. J.; Coronado, E. Enhanced superconductivity in atomically thin TaS_2. *Nat. Commun.* **2016**, *7*, 11043.
(25) de la Barrera, S. C.; Sinko, M. R.; Gopalan, D. P.; Sivadas, N.; Seyler, K. L.; Watanabe, K.; Taniguchi, T.; Tsen, A. W.; Xu, X.; Xiao, D.; Hunt, B. M. Tuning Ising superconductivity with layer and spin−orbit coupling in two-dimensional transition-metal dichalcogenides. *Nat. Commun.* **2018**, *9*, 1427.
(26) Chang, K.; Liu, J.; Lin, H.; Wang, N.; Zhao, K.; Zhang, A.; Jin, F.; Zhong, Y.; Hu, X.; Duan, W.; Zhang, Q.; Fu, L.; Xue, Q.-K.; Chen, X.; Ji, S.-H. Discovery of robust in-plane ferroelectricity in atomic-thick SnTe. *Science* **2016**, *353*, 274−278.
(27) Fei, Z.; Zhao, W.; Palomaki, T. A.; Sun, B.; Miller, M. K.; Zhao, Z.; Yan, J.; Xu, X.; Cobden, D. H. Ferroelectric switching of a two-dimensional metal. *Nature* **2018**, *560*, 336−339.
(28) Xi, X.; Zhao, L.; Wang, Z.; Berger, H.; Forró, L.; Shan, J.; Mak, K. F. Strongly enhanced charge-density-wave order in monolayer $NbSe_2$. *Nat. Nanotechnol.* **2015**, *10*, 765.
(29) Zhang, R.; Willis, R. F. Thickness-dependent curie temperatures of ultrathin magnetic films: Effect of the range of spin-spin interactions. *Phys. Rev. Lett.* **2001**, *86*, 2665−2668.
(30) Li, Y.; Baberschke, K. Dimensional crossover in ultrathin Ni(111) films on W(110). *Phys. Rev. Lett.* **1992**, *68*, 1208−1211.
(31) Qiu, Z. Q.; Pearson, J.; Bader, S. D. Asymmetry of the spin reorientation transition in ultrathin Fe films and wedges grown on Ag(100). *Phys. Rev. Lett.* **1993**, *70*, 1006−1009.
(32) Schneider, C. M.; Bressler, P.; Schuster, P.; Kirschner, J.; de Miguel, J. J.; Miranda, R. Curie temperature of ultrathin films of fcc-cobalt epitaxially grown on atomically flat Cu(100) surfaces. *Phys. Rev. Lett.* **1990**, *64*, 1059−1062.
(33) Jiang, J. S.; Davidović, D.; Reich, D. H.; Chien, C. L. Oscillatory superconducting transition temperature in Nb/Gd multilayers. *Phys. Rev. Lett.* **1995**, *74*, 314−317.

https://dx.doi.org/10.1021/acs.nanolett.9b05128
Nano Lett. 2020, 20, 3130−3139

(34) Liu, Y.; Petrovic, C. Critical behavior of the quasi-two-dimensional weak itinerant ferromagnet trigonal chromium telluride $Cr_{0.62}Te$. *Phys. Rev. B: Condens. Matter Mater. Phys.* **2017**, *96*, 134410.
(35) Tongay, S.; Varnoosfaderani, S. S.; Appleton, B. R.; Wu, J.; Hebard, A. F. Magnetic properties of MoS_2: Existence of ferromagnetism. *Appl. Phys. Lett.* **2012**, *101*, 123105.
(36) Cervenka, J.; Katsnelson, M. I.; Flipse, C. F. J. Room-temperature ferromagnetism in graphite driven by two-dimensional networks of point defects. *Nat. Phys.* **2009**, *5*, 840.
(37) Wang, J.; Sun, F.; Yang, S.; Li, Y.; Zhao, C.; Xu, M.; Zhang, Y.; Zeng, H. Robust ferromagnetism in Mn-doped MoS_2 nanostructures. *Appl. Phys. Lett.* **2016**, *109*, 092401.
(38) Nagaosa, N.; Sinova, J.; Onoda, S.; MacDonald, A. H.; Ong, N. P. Anomalous Hall effect. *Rev. Mod. Phys.* **2010**, *82*, 1539−1592.
(39) Jiang, Z.; Wang, P.; Xing, J.; Jiang, X.; Zhao, J. Screening and design of novel 2D ferromagnetic materials with high curie temperature above room temperature. *ACS Appl. Mater. Interfaces* **2018**, *10*, 39032−39039.
(40) Zhu, Y.; Kong, X.; Rhone, T. D.; Guo, H. Systematic search for two-dimensional ferromagnetic materials. *Phys. Rev. Mater.* **2018**, *2*, 081001.
(41) Anderson, P. W. Theory of magnetic exchange interactions - exchange in insulators and semiconductors. *Solid State Phys.* **1963**, *14*, 99−214.
(42) Şaşıoğlu, E.; Sandratskii, L. M.; Bruno, P. First-principles calculation of the intersublattice exchange interactions and Curie temperatures of the full Heusler alloys Ni_2MnX (X = Ga,In,Sn,Sb). *Phys. Rev. B: Condens. Matter Mater. Phys.* **2004**, *70*, 024427.
(43) Kresse, G.; Furthmüller, J. Efficient iterative schemes for ab initio total-energy calculations using a plane-wave basis set. *Phys. Rev. B: Condens. Matter Mater. Phys.* **1996**, *54*, 11169−11186.
(44) Blöchl, P. E. Projector augmented-wave method. *Phys. Rev. B: Condens. Matter Mater. Phys.* **1994**, *50*, 17953−17979.
(45) Perdew, J. P.; Burke, K.; Ernzerhof, M. Generalized gradient approximation made simple. *Phys. Rev. Lett.* **1996**, *77*, 3865−3868.
(46) Liechtenstein, A. I.; Anisimov, V. I.; Zaanen, J. Density-functional theory and strong interactions: Orbital ordering in Mott-Hubbard insulators. *Phys. Rev. B: Condens. Matter Mater. Phys.* **1995**, *52*, R5467−R5470.
(47) Zhang, J.; Zhao, B.; Zhou, T.; Xue, Y.; Ma, C.; Yang, Z. Strong magnetization and Chern insulators in compressed graphene/CrI_3 van der Waals heterostructures. *Phys. Rev. B: Condens. Matter Mater. Phys.* **2018**, *97*, 085401.
(48) Monkhorst, H. J.; Pack, J. D. Special points for Brillouin-zone integrations. *Phys. Rev. B* **1976**, *13*, 5188−5192.
(49) Xiong, W.; Xia, C.; Du, J.; Wang, T.; Zhao, X.; Peng, Y.; Wei, Z.; Li, J. Electrostatic gating dependent multiple-band alignments in a high-temperature ferromagnetic $Mg(OH)_2/VS_2$ heterobilayer. *Phys. Rev. B: Condens. Matter Mater. Phys.* **2017**, *95*, 245408.
(50) Zhou, J.; Wang, Q.; Sun, Q.; Jena, P. Electronic and magnetic properties of a BN sheet decorated with hydrogen and fluorine. *Phys. Rev. B: Condens. Matter Mater. Phys.* **2010**, *81*, 085442.

https://dx.doi.org/10.1021/acs.nanolett.9b05128
Nano Lett. 2020, 20, 3130−3139